

Spin transport in a charge current induced magnon Bose-Einstein condensate at room temperature

T. Wimmer,^{1,2,*} M. Althammer,^{1,2,†} L. Liensberger,^{1,2} N. Vlietstra,¹
S. Geprägs,¹ M. Weiler,^{1,2} R. Gross,^{1,2,3} and H. Huebl^{1,2,3,‡}

¹Walther-Meißner-Institut, Bayerische Akademie der Wissenschaften, 85748 Garching, Germany

²Physik-Department, Technische Universität München, 85748 Garching, Germany

³Nanosystems Initiative Munich (NIM), Schellingstraße 4, 80799 München, Germany

(Dated: August 8, 2022)

Bose-Einstein condensation (BEC) describes a state of matter in which identical particles with integer angular momentum (bosons) occupy a collective quantum state [1, 2]. BEC is at the heart of many macroscopic quantum phenomena, including superfluidity [3], the condensation of diluted gas systems [4] as well as of bosonic excitations in solid-state systems [5–8]. Most importantly, BEC is the key prerequisite for dissipationless transport phenomena, forming the basis for quantum technologies on many levels. The magnetic analogon, the magnon BEC, is particularly appealing for applications, as it can emerge at room temperature [8]. However, transport phenomena within the magnon condensate or the generation of a critical magnon density by DC charge currents have only been considered theoretically [9–11]. Here, we demonstrate the realization of magnon BEC using a DC magnetotransport scheme and study its room temperature magnon conductivity. Above a critical magnon density, the magnon conductivity increases by almost two orders of magnitude, indicating dissipationless magnon transport, i.e. the realization of spin superfluidity [12]. Our results demonstrate an all-electrical approach for the investigation of spin transport in a magnon condensate. The regime of dissipationless magnon transport paves the way for phenomena equivalent to Josephson effects in superconductivity and will be of key relevance for future (quantum) magnonic devices.

The phenomenon of BEC is inherently connected to the quantum statistics of bosons. When lowering the temperature at constant boson density, the chemical potential μ approaches the energy of the ground state and the latter becomes macroscopically populated. Considering bosonic excitations in a solid, such as phonons or magnons, BEC cannot be realized in a thermal equilibrium situation, since the boson number is not conserved ($\mu = 0$). The boson number rather decreases with decreasing temperature as, loosely speaking, the excitations freeze out. Continuous generation of excitations by external pumping, however, results in a steady-state non-equilibrium situation with finite μ [13, 14]. Such driven BEC has been reported for many systems such as excitons [5], phonons [6], photons [7] and magnons [8]. For the latter, BEC was achieved using a two-magnon excitation scheme followed by a thermal relaxation of the magnons into the ground state [8]. Recently, Bender et al. [9] suggested the creation of magnon BEC by injection of a DC spin current into a magnetic material, resulting in a steady-state non-equilibrium with finite magnon chemical potential μ_m [14]. When μ_m exceeds a critical value, the ground state becomes macroscopically populated and BEC is achieved. In our corresponding experiments [15], we realize spin current injection into a magnetic insulator (MI) via the spin Hall effect (SHE) [16, 17] by driving a charge current I_{dc} through a heavy metal

(HM) strip in contact with the MI. As a result, a spin chemical potential $\mu_s = \frac{e\theta_{SH}I_{dc}}{w\sigma_e\eta} \tanh(\eta)$ [14, 18, 19] builds up at the HM/MI interface, leading to a non-equilibrium magnon density in the MI. Here, e is the elementary charge, w denotes the width of the HM strip, σ_e and θ_{SH} are the electric conductivity and the spin Hall angle of the HM. Moreover, $\eta = t_{HM}/(2l_s)$ is the ratio of the thickness of the HM strip t_{HM} and its spin diffusion length l_s . Since μ_m is expected to grow with μ_s , we can tune μ_m by varying I_{dc} . Adopting the model in Ref. [9] to our experimental configuration, the criteria for the formation of magnon BEC as well as the swasing instability (the spin wave analogon of lasing [20]) within the DC pumped magnon condensate are given by

$$\mu_{BEC/SW} = \left(1 + \frac{\alpha_{eff}}{c \cdot \alpha_{sp}}\right) \left[\hbar\gamma\mu_0 \left(H + \frac{M_s}{2}\right)\right]. \quad (1)$$

Here, $\mu_s = \mu_{BEC}$ (i.e. $I_{dc} = I_{BEC}$) corresponds to the critical spin chemical potential (current) for the formation of magnon BEC with $c = 2$, while $\mu_s = \mu_{SW}$ (i.e. $I_{dc} = I_{SW}$) corresponds to the swasing instability with $c = 1$. Furthermore, α_{eff} is an effective damping parameter (see SI), α_{sp} is the spin pumping induced damping enhancement of the MI, \hbar is the reduced Planck constant, γ is the gyromagnetic ratio and μ_0 is the vacuum permeability. The criteria further depend on the external magnetic field H and the saturation magnetization M_s . As magnon BEC represents a state of coherent magnetization precession, it resembles the classical phenomenon of spin torque oscillators [21]. Here, the threshold criterion is determined by the frequency linewidth

* tobias.wimmer@wmi.badw.de

† matthias.althammer@wmi.badw.de

‡ hans.huebl@wmi.badw.de

(damping rate) of the ferromagnetic resonance (FMR) transition. As detailed in the SI, we find full equivalence of the DC current pumped magnon swasing criterion [9] (μ_{SW} in Eq. (1)) and the DC current threshold for spin torque auto-oscillations, which is the classical description of swasing.

In this letter, we report on magnon transport properties across the phase transition of a DC pumped magnon Bose-Einstein condensate formed in the ferrimagnetic insulator yttrium iron garnet (YIG). Within the swasing phase of the magnon condensate, we find an increased magnon conductivity by almost two orders of magnitude, indicating dissipationless transport of magnons.

The principle of our magnon conductance measurement is inspired by recent DC magnetotransport experiments that infer magnon properties in YIG [14, 15, 22–26]. Here, magnons are injected from a Pt strip (injector) into the YIG by a low-frequency (13 Hz) charge current I_{ac} (see Fig. 1a) and the SHE in Pt. The diffusion and, hence, the conductivity of these magnons is quantified by electrically measuring the magnon density below a second Pt strip (detector) as a voltage signal V_{ac} exploiting the inverse SHE. Cornelissen et al. [27] demonstrated that the magnon conductivity measured in such an arrangement can be controlled by a DC charge current I_{dc} applied to a third (modulator) strip placed between injector and detector. In a simple picture, I_{dc} controls the magnon density below the modulator and thereby alters the magnon conductivity.

In contrast to Ref. [27], we here focus on the non-linear regime of this magnon conductance. Our physical picture of the the magnon transport beneath the modulator is condensed in Fig. 1: For $I_{\text{dc}} = 0$ (panel b), the magnon density n_{m}^{ac} from the injector decays exponentially (orange solid line). For $I_{\text{dc}} = I_{\text{BEC}}$ (panel c), the magnon density generated by the modulator is sufficient to support the formation of magnon BEC. Due to the strong increase in magnon density for $I_{\text{dc}} \gtrsim I_{\text{BEC}}$, the magnon conductivity is enhanced, which results in an increased V_{ac} at the detector. For $I_{\text{dc}} = I_{\text{SW}}$ (panel d), the swasing threshold of the magnon BEC state is reached, the magnon lifetime diverges and a macroscopic excitation is generated. In this swasing state, the magnon damping is completely compensated by the DC pumping and dissipationless transport ensues.

To investigate the magnon propagation in the YIG for different modulator currents I_{dc} and to test the criteria set in Eq. (1), we measure V_{ac} as a function of the magnetic field orientation φ with a fixed magnetic field strength of $\mu_0 H = 50 \text{ mT}$ at a temperature $T = 280 \text{ K}$. The result is shown in Fig. 2, where the black data points show the characteristic ($\cos^2 \varphi$) modulation expected for magnon transport between injector and detector for $I_{\text{dc}} = 0$, resulting from the variation of the magnon injection with φ with maxima expected for H perpendicular to I_{ac} ($\varphi = -180^\circ, 0^\circ, 180^\circ$) [15, 22]. Interestingly, a significant enhancement of the magnon transport signal is observed at $\varphi = \pm 180^\circ$ in Fig. 2a for

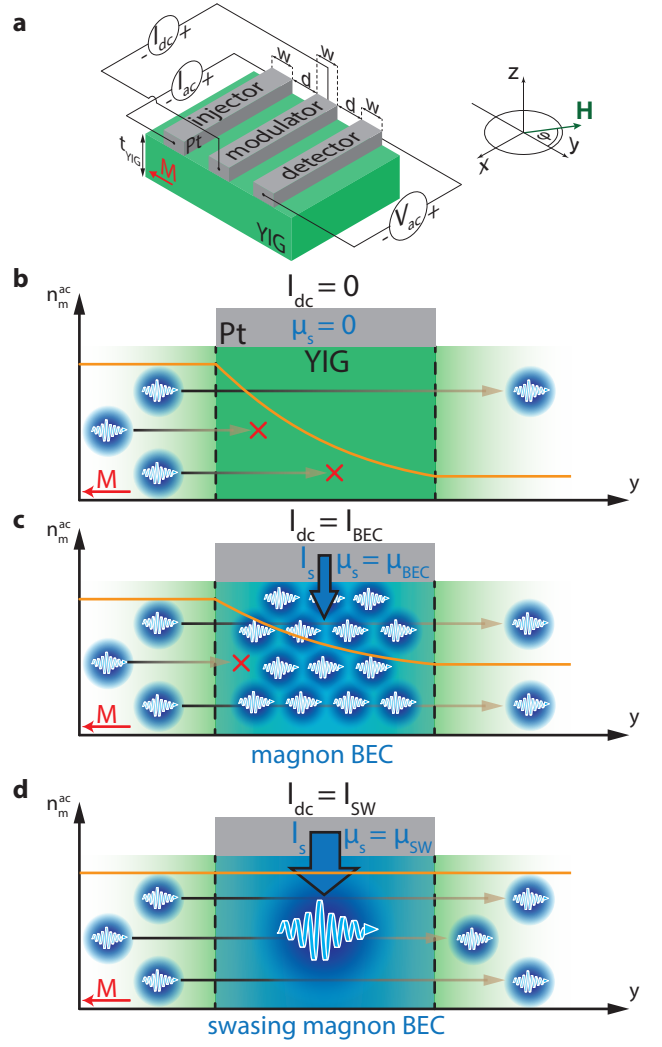


Figure 1. **a** Schematic depiction of the device, electrical connection scheme and the coordinate system. **b**, **c**, **d** Illustrations of the magnon transport from injector to detector. We here only consider magnon transport directly below the modulator. **b** For $I_{\text{dc}} = 0$, magnons (blue wiggly arrows) generated by the injector diffuse from left to right. Scattering events, indicated by red crosses, result in a finite lifetime and a corresponding characteristic spin diffusion length depicted as an exponential decay of the magnon density n_{m}^{ac} (orange solid line). The modulator only statically affects the transport properties via magnon absorption. **c** For $I_{\text{dc}} = I_{\text{BEC}}$, the magnon density beneath the modulator reaches the threshold for the formation of magnon BEC with a strong non-linear increase of the conductance for $I_{\text{dc}} \gtrsim I_{\text{BEC}}$. **d** For $I_{\text{dc}} = I_{\text{SW}}$, the magnon condensate enters the swasing regime, where the effective damping of the magnons is fully compensated. This results in dissipationless magnon transport beneath the modulator.

$I_{\text{dc}} > 0$. This can be understood by a magnon accumulation underneath the modulator, which increases the magnon conductivity and results in a larger V_{ac} . In the same way, a decrease of V_{ac} is expected for $\varphi = 0^\circ$ due to the magnon depletion obtained in this configuration.

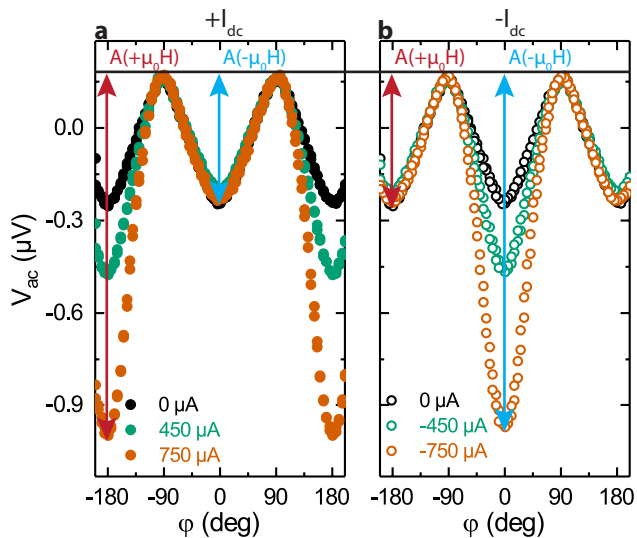


Figure 2. Detector signal V_{ac} for in-plane magnetic field rotations at $\mu_0 H = 50$ mT for (a) positive and (b) negative bias currents in the modulator. **a** The magnon transport signal for $I_{dc} > 0$ is significantly increased at $\varphi = \pm 180^\circ$ and mostly unaffected at $\varphi = 0^\circ$. **b** For $I_{dc} < 0$, we observe the expected, by 180° shifted behavior, where the signal increase is evident at $\varphi = 0^\circ$, while unchanged for $\varphi = \pm 180^\circ$.

However, this is counterbalanced by thermally injected magnons present due to Joule heating of the modulator strip. Figure 2b shows the measurement for the inverted DC current direction ($I_{dc} < 0$). Here, we observe the expected 180° shifted case: an enhancement for $\varphi = 0^\circ$ and no significant change for $\pm 180^\circ$. This behaviour is consistent with an accumulation of magnons for the given current and magnetic field direction.

For a quantitative analysis of the data presented in Fig. 2, we extract the amplitudes $A(+\mu_0 H)$ and $A(-\mu_0 H)$ as a function of I_{dc} for various magnetic field amplitudes H (see Fig. 3). In the low bias regime ($|I_{dc}| < 0.4$ mA), the $A(I_{dc})$ curves can be modeled by a superposition of a linear and quadratic dependence as already reported by Cornelissen et al. [27] (see SI). However, we observe a two orders of magnitude improved control of the magnon conductivity compared to Ref. [27]. This is in agreement with the predicted magnetic layer thickness dependence of the modulation efficiency [27]. A quantitative comparison to the model of Ref. [27] is shown in the SI. In addition, and most importantly, we see a pronounced deviation from the linear in I_{dc} transport modulation [27] for large I_{dc} . This manifests itself by a shoulder in the $A(I_{dc})$ curves for $I_{dc} > 0.5$ mA (marked by black triangles).

We now focus on the magnon transport properties, i.e. the magnon resistance R_{YIG}^s . To this end, we evaluate the magnon resistance measured between injector and detector as a function of the modulator current. As explained in detail in the methods, the spin resistance in YIG can be directly deduced from the magnon trans-

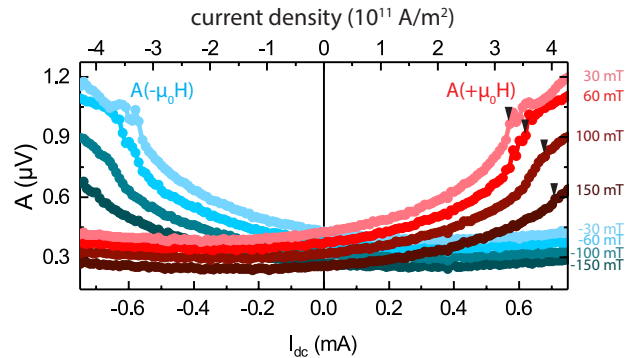


Figure 3. Extracted amplitudes $A(+\mu_0 H)$ and $A(-\mu_0 H)$ (as indicated in Fig. 2) of the magnon transport signal for different external magnetic fields plotted versus the dc current I_{dc} in the modulator. The phase transition into swasing magnon BEC for positive I_{dc} is indicated by black triangles (maximum slope of the curves). The transition shifts to larger DC currents with increasing external magnetic fields.

port amplitudes A plotted in Fig. 3 [14]. However, A contains contributions from thermal (quadratic in I_{dc}) as well as SHE induced injection effects (linear in I_{dc}). We correct for both of those contributions, leading to the $R_{YIG}^s(I_{dc})$ dependence shown in Fig. 4a (details are given in the SI). Thus, $R_{YIG}^s(I_{dc})$ enables us to evidence the impact on magnon transport stemming solely from magnon BEC and swasing. For $I_{dc} < 0.4$ mA, we observe a constant R_{YIG}^s . At the characteristic current I_{BEC} , the magnon resistance R_{YIG}^s starts to drop rapidly by 0.13Ω and saturates at a finite value above the second characteristic current I_{SW} . Here, we define I_{BEC} as the current at which R_{YIG}^s drops by 10% compared to the constant resistance observed for small I_{dc} . I_{SW} is taken at the current level where R_{YIG}^s reaches its minimum value.

In Fig. 4b, the experimentally determined critical currents I_{BEC} and I_{SW} are plotted as a function of the applied magnetic field. For I_{BEC} (I_{SW}), we observe a critical current around 0.45 mA (0.6 mA) for $\mu_0 H < 50$ mT and both critical currents increase with the applied magnetic field strength for $\mu_0 H > 50$ mT. We can understand this behaviour quantitatively by solving the aforementioned condition $\mu_s = \mu_{BEC}$ ($\mu_s = \mu_{SW}$) for I_{dc} . Using the values $\sigma_e = 1.74 \times 10^6$ 1/ Ω m, $\theta_{SH} = 0.11$, $l_s = 1.5$ nm, $w = 500$ nm and $t_{Pt} = 3.5$ nm to calculate μ_s , we find excellent quantitative agreement of model and experimental data for both I_{SW} (spheres and red line) and I_{BEC} (stars and blue line). The characteristic parameters α_{eff} and α_{sp} entering Eq. (1) are determined independently using ferromagnetic resonance experiments presented in the SI. We want to emphasize that the magnetic field dependence of I_{SW} is identical to the critical current dependence for auto-oscillations in spin Hall nano-oscillators [21] (see SI). It is remarkable that we observe the spin torque auto-oscillations without any patterning of the YIG. The geometrical confinement required for stable spin torque oscillations is rather de-

terminated solely by the geometry of the Pt strip.

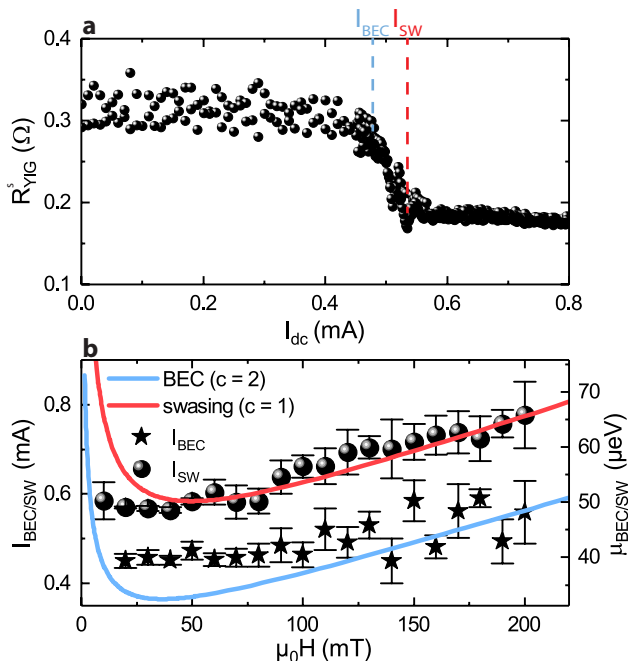


Figure 4. **a** Magnon resistance R_{YIG}^s of the YIG channel between injector and detector for a magnetic field of $\mu_0 H = 50$ mT. The magnon resistance is corrected for effects associated with linear SHE and thermal magnon injection effects (see SI). A very steep decrease of R_{YIG}^s for $I_{\text{BEC}} < I_{\text{dc}} < I_{\text{SW}}$ is evident. The reduction of R_{YIG}^s by 0.13Ω is compatible with a vanishing magnon resistivity underneath the modulator strip. **b** Critical currents $I_{\text{BEC/SW}}$ versus applied field $\mu_0 H$. The right y -axis shows the critical chemical potentials $\mu_{\text{BEC/SW}}$ from Eq. (1) (solid red and blue lines).

The spin resistance data (Fig. 4a) also allows us to roughly estimate the condensate resistance within the swasing phase. Assuming a serial resistor network model [14] (see SI), and zero magnon resistance underneath the modulator strip when the swasing condensate is formed, we expect $R_{\text{YIG}}^s = 0.19 \Omega$ for $I_{\text{dc}} > I_{\text{SW}}$, which is in excellent agreement with our data shown in Fig. 4a. We can further roughly estimate the spin resistivity ρ_{YIG}^s for the swasing magnon condensate and obtain $8.16 \text{ n}\Omega \text{ m}$, which is almost two orders of magnitude smaller than the spin resistivity in the normal state ($0.54 \mu\Omega \text{ m}$) (see SI). Thus, the observed spin resistance shows similarities to the sudden electrical resistance drop of a superconductor at the superconducting phase transition. Our data therefore provides evidence for the presence of a magnon BEC state with vanishing spin resistivity, which is also known as spin superfluidity [10–12, 28]. The observation of a magnon conductivity change in the BEC swasing regime warrants the question how a coherent magnetization precession induced by ferromagnetic resonance affects the transport properties. In stark contrast to the reduction

of spin resistance due to the formation of the BEC, we find an increase of spin resistance when coherently driving the YIG magnetization by a low power microwave magnetic field (see SI) [29]. This demonstrates that the effective compensation of magnetic damping in the BEC phase is responsible for the formation of the superfluid - and not the coherent magnetization precession.

The excellent quantitative agreement between our experimental data and the model predicting BEC/swasing by DC spin current injection into magnetic insulators by Bender et al. [9] strongly suggests the formation of BEC in the YIG thin film. This transition from a classical magnon gas into a collective quantum state can also be independently estimated by comparing the thermal de Broglie wavelength Λ with the mean (magnon) particle distance a . While for $a \gg \Lambda$ the particles form a classical gas, a degenerate quantum gas is obtained for $a \lesssim \Lambda$. We estimate the induced magnon density n_m via spin-orbit torque, as pursued in this experiment, to be $10^{23}/\text{cm}^3$ for $I_{\text{dc}} = 0.8 \text{ mA}$ (see SI). In comparison, the thermal magnon de Broglie wavelength at room temperature is $\sim 2 \text{ nm}$, which exceeds the mean particle separation $a \approx n_m^{-1/3} \approx 0.2 \text{ nm}$ by an order of magnitude (see SI). Thus, even this simple estimate strongly supports the formation of a magnon Bose-Einstein condensate.

In summary, we find ultra-low magnon resistance indicating superfluid spin transport through the swasing phase of a DC pumped magnon condensate. Here, BEC is created by employing spin-orbit torque mediated spin current injection in a YIG/Pt heterostructure. We find excellent quantitative agreement between our experimental data and the theoretically predicted threshold conditions for the transition into magnon BEC and the swasing instability of the magnon BEC [9]. This work lays the foundation for experiments ranging from zero-resistance magnon transport to physics equivalent to the Josephson effects in superconductivity [10, 30]. Eventually, it even has the potential to make a significant impact on modern day magnon based (quantum) devices.

ACKNOWLEDGMENTS

T.W. acknowledges Akashdeep Kamra for valuable discussions. This work is financially supported by the DFG via projects AL2110/2-1, WE5386/4-1 and HU1896/2-1.

AUTHOR CONTRIBUTIONS

T.W., M.A., L.L. and N.V. carried out the experiments and evaluated the data. T.W. fabricated the sample. S.G. performed the thin film growth. H.H., M.A. and R.G. supervised the project. T.W., M.A., M.W., R.G., H.H. and S.G. interpreted the results. T.W., M.A., M.W. and H.H. prepared the manuscript and figures with the assistance of all authors.

- [1] Bose, S. Plancks Gesetz und Lichtquantenhypothese. *Zeitschrift für Physik* **26**, 178–181 (1924). URL <https://doi.org/10.1007/BF01327326>.
- [2] Einstein, A. Quantentheorie des einatomigen idealen Gases. Zweite Abhandlung. In *Albert Einstein: Akademie-Vorträge*, 245–257 (Wiley-VCH Verlag GmbH & Co. KGaA, 2006). URL <https://doi.org/10.1002/3527608958.ch28>.
- [3] Halperin, W. P. Eighty years of superfluidity. *Nature* **553**, 413–414 (2018). URL <https://doi.org/10.1038/d41586-018-00417-7>.
- [4] Bloch, I., Dalibard, J. & Zwirger, W. Many-body physics with ultracold gases. *Reviews of Modern Physics* **80**, 885–964 (2008). URL <https://doi.org/10.1103/revmodphys.80.885>.
- [5] Eisenstein, J. P. & MacDonald, A. H. Bose-Einstein condensation of excitons in bilayer electron systems. *Nature* **432**, 691–694 (2004). URL <https://doi.org/10.1038/nature03081>.
- [6] Misochko, O., Hase, M., Ishioka, K. & Kitajima, M. Transient Bose-Einstein condensation of phonons. *Physics Letters A* **321**, 381–387 (2004). URL <https://doi.org/10.1016/j.physleta.2003.11.063>.
- [7] Klaers, J., Schmitt, J., Vewinger, F. & Weitz, M. Bose-Einstein condensation of photons in an optical microcavity. *Nature* **468**, 545–548 (2010). URL <https://doi.org/10.1038/nature09567>.
- [8] Demokritov, S. O. *et al.* Bose-einstein condensation of quasi-equilibrium magnons at room temperature under pumping. *Nature* **443**, 430–433 (2006). URL <https://doi.org/10.1038/nature05117>.
- [9] Bender, S. A., Duine, R. A., Brataas, A. & Tserkovnyak, Y. Dynamic phase diagram of depumped magnon condensates. *Physical Review B* **90**, 094409 (2014). URL <https://link.aps.org/doi/10.1103/PhysRevB.90.094409>.
- [10] Skarsvåg, H., Holmqvist, C. & Brataas, A. Spin superfluidity and long-range transport in thin-film ferromagnets. *Physical Review Letters* **115**, 237201 (2015). URL <https://link.aps.org/doi/10.1103/PhysRevLett.115.237201>.
- [11] Qaiumzadeh, A., Skarsvåg, H., Holmqvist, C. & Brataas, A. Spin superfluidity in biaxial antiferromagnetic insulators. *Physical Review Letters* **118**, 137201 (2017). URL <https://link.aps.org/doi/10.1103/PhysRevLett.118.137201>.
- [12] Bozhko, D. A. *et al.* Supercurrent in a room-temperature bose-einstein magnon condensate. *Nature Physics* **12**, 1057–1062 (2016). URL <https://doi.org/10.1038/nphys3838>.
- [13] Fröhlich, H. Bose condensation of strongly excited longitudinal electric modes. *Physics Letters A* **26**, 402 – 403 (1968). URL <http://www.sciencedirect.com/science/article/pii/0375960168902429>.
- [14] Cornelissen, L. J., Peters, K. J. H., Bauer, G. E. W., Duine, R. A. & van Wees, B. J. Magnon spin transport driven by the magnon chemical potential in a magnetic insulator. *Physical Review B* **94**, 014412 (2016). URL <http://link.aps.org/doi/10.1103/PhysRevB.94.014412>.
- [15] Goennenwein, S. T. B. *et al.* Non-local magnetoresistance in yig/pt nanostructures. *Applied Physics Letters* **107**, 172405 (2015). URL <http://scitation.aip.org/content/aip/journal/apl/107/17/10.1063/1.4935074>.
- [16] Hirsch, J. E. Spin Hall Effect. *Physical Review Letters* **83**, 1834–1837 (1999). URL <http://link.aps.org/doi/10.1103/PhysRevLett.83.1834>.
- [17] Dyakonov, M. I. & Perel, V. I. Possibility of orienting electron spins with current. *Journal of Experimental and Theoretical Physics Letters* **13** (1971).
- [18] Chen, Y.-T. *et al.* Theory of spin hall magnetoresistance. *Physical Review B* **87**, 144411 (2013). URL <http://link.aps.org/doi/10.1103/PhysRevB.87.144411>.
- [19] Zhang, S. S.-L. & Zhang, S. Spin convertance at magnetic interfaces. *Physical Review B* **86**, 214424 (2012). URL <http://link.aps.org/doi/10.1103/PhysRevB.86.214424>.
- [20] Berger, L. Emission of spin waves by a magnetic multilayer traversed by a current. *Physical Review B* **54**, 9353–9358 (1996). URL <https://doi.org/10.1103/physrevb.54.9353>.
- [21] Collet, M. *et al.* Generation of coherent spin-wave modes in yttrium iron garnet microdiscs by spin-orbit torque. *Nature Communications* **7**, 10377 (2016). URL <https://doi.org/10.1038/ncomms10377>.
- [22] Cornelissen, L. J., Liu, J., Duine, R. A., Youssef, J. B. & van Wees, B. J. Long-distance transport of magnon spin information in a magnetic insulator at room temperature. *Nature Physics* **11**, 1022–1026 (2015). URL <https://doi.org/10.1038/nphys3465>.
- [23] Ganzhorn, K. *et al.* Magnon-based logic in a multi-terminal YIG/pt nanostructure. *Applied Physics Letters* **109**, 022405 (2016). URL <https://doi.org/10.1063/1.4958893>.
- [24] Thiery, N. *et al.* Nonlinear spin conductance of yttrium iron garnet thin films driven by large spin-orbit torque. *Physical Review B* **97**, 060409 (2018). URL <https://link.aps.org/doi/10.1103/PhysRevB.97.060409>.
- [25] Althammer, M. Pure spin currents in magnetically ordered insulator/normal metal heterostructures. *Journal of Physics D: Applied Physics* **51**, 313001 (2018). URL <https://doi.org/10.1088/1361-6463/aaca89>.
- [26] Lebrun, R. *et al.* Tunable long-distance spin transport in a crystalline antiferromagnetic iron oxide. *Nature* **561**, 222–225 (2018). URL <https://doi.org/10.1038/s41586-018-0490-7>.
- [27] Cornelissen, L. J., Liu, J., van Wees, B. J. & Duine, R. A. Spin-current-controlled modulation of the magnon spin conductance in a three-terminal magnon transistor. *Physical Review Letters* **120**, 097702 (2018). URL <https://link.aps.org/doi/10.1103/PhysRevLett.120.097702>.
- [28] Takei, S. & Tserkovnyak, Y. Superfluid spin transport through easy-plane ferromagnetic insulators. *Physical Review Letters* **112** (2014). URL <https://doi.org/10.1103/physrevlett.112.227201>.
- [29] Liu, J. *et al.* Microwave control of thermal magnon spin transport. *ArXiv e-prints* (2018). URL <https://arxiv.org/abs/1810.11667>.

- [30] Nakata, K., van Hoogdalem, K. A., Simon, P. & Loss, D. Josephson and persistent spin currents in Bose-Einstein condensates of magnons. *Physical Review B* **90**, 144419 (2014). URL <https://link.aps.org/doi/10.1103/PhysRevB.90.144419>.

METHODS

Sample preparation

The 13.4 nm thick, single crystalline (100)-oriented yttrium iron garnet ($\text{Y}_3\text{Fe}_5\text{O}_{12}$, YIG) film was grown via pulsed laser deposition at the Walther-Meißner-Institute on a gadolinium gallium garnet ($\text{Gd}_3\text{Ga}_5\text{O}_{12}$, GGG) substrate using a substrate temperature of 450 °C, an oxygen pressure of 25 μbar , a laser fluence at the target of 2.0 J/cm² and a laser frequency of 10 Hz. The YIG film exhibits a saturation magnetization of 140 mT and a Gilbert damping of 2×10^{-3} . The 3.5 nm thick Pt strips were deposited on the YIG thin film by DC sputtering and were patterned by e-beam lithography: the strips have an edge-to-edge separation of $d = 400$ nm and a width of $w = 500$ nm. Subsequently, Ti/Al layers of 5/50 nm were deposited on the film by DC sputtering and patterned into leads for the Pt strips to contact the device electrically. A low frequency ($f = 13.131$ Hz) AC current I_{ac} of 50 μA is fed through the injector with a Keithley 6221 current source. To detect the magnon conductivity, we measure the first harmonic SHE voltage V_{ac} at the detector strip using a Zurich Instruments HF2LI lock-in amplifier. The voltage signal is preamplified by a Stanford Research Systems SR560 low-noise voltage amplifier before being passed to the lock-in. In addition, we

vary the DC current I_{dc} applied to the modulator strip with a Keithley 2400 Sourcemeter to control the magnon chemical potential. The use of this lock-in detection technique is essential to distinguish between magnons stemming from the DC driven modulator and the AC driven injector [23, 27].

YIG spin resistance

The spin resistance $R_{\text{YIG}}^{\text{s}}$ in YIG was determined by adopting an equivalent spin-resistor model [14]:

$$R_{\text{YIG}}^{\text{s}} = \frac{R_{\text{Pt}}^{\text{s}}}{\eta_{\text{s}}} - (2R_{\text{int}}^{\text{s}} + 2R_{\text{Pt}}^{\text{s}}), \quad (2)$$

where $R_{\text{Pt}}^{\text{s}} = l_{\text{s}}/(\sigma_{\text{e}}A_{\text{int}}\tanh(t_{\text{Pt}}/l_{\text{s}}))$ is the spin resistance of the Pt strip and $R_{\text{int}}^{\text{s}} = 1/(g_{\text{s}}A_{\text{int}})$ the interface spin resistance. We will neglect the last two terms in Eq. (2) (i.e. the interface and Pt spin resistances), since these are three orders of magnitude smaller than the first term. η_{s} denotes the spin transfer efficiency from injector to detector and reads

$$\eta_{\text{s}} = \frac{t_{\text{Pt}}}{l_{\text{s}}\theta_{\text{SH}}^2} \frac{A_{\text{corr}}}{I_{\text{ac}}R_{\text{det}}} \frac{(e^{t_{\text{Pt}}/l_{\text{s}}} + 1)(e^{2t_{\text{Pt}}/l_{\text{s}}} + 1)}{(e^{t_{\text{Pt}}/l_{\text{s}}} - 1)^3} \quad (3)$$

with R_{det} the electrical resistance of the Pt detector strip. In order to isolate the effect of the magnon BEC on the spin resistance, we use the corrected voltage amplitudes A_{corr} (see SI) of the magnon transport signal for the calculation of η_{s} and eventually of $R_{\text{YIG}}^{\text{s}}$.